Rapid neurotransmitter uncaging in spatially defined patterns

Shy Shoham[1,2,4,5], Daniel H O'Connor[1,2,5], Dmitry V Sarkisov[2,3] & Samuel S-H Wang[1,2]

Light-sensitive 'caged' molecules provide a means of rapidly and noninvasively manipulating biochemical signals with submicron spatial resolution. Here we describe a new optical system for rapid uncaging in arbitrary patterns to emulate complex neural activity. This system uses TeO_2 acousto-optical deflectors to steer an ultraviolet beam rapidly and can uncage at over 20,000 locations per second. The uncaging beam is projected into the focal plane of a two-photon microscope, allowing us to combine patterned uncaging with imaging and electrophysiology. By photolyzing caged neurotransmitter in brain slices we can generate precise, complex activity patterns for dendritic integration. The method can also be used to activate many presynaptic neurons at once. Patterned uncaging opens new vistas in the study of signal integration and plasticity in neuronal circuits and other biological systems.

Neurons integrate synaptic signals from many thousands of inputs. Understanding the resulting information processing is a central theme in experimental and computational neuroscience. Multiple inputs can interact to amplify[1], attenuate[2] or modulate one another. Thus, results obtained by activating one or a few inputs at a time, as is commonly done in brain slice experiments, do not fully capture the complexity of signal processing by single neurons.

This potential complexity of signal integration suggests the need to manipulate biochemical and electrical events across dendrites and in multiple neurons with fine spatial and temporal resolution. An attractive option for performing such manipulations is the use of optical approaches in the form of photochemical release of caged neurotransmitters and second messengers[3,4]. In optical uncaging, a biologically active molecule is inactivated through covalent attachment of a caging group, is introduced into tissue and is then converted to its active form by a flash of light. A large variety of caged compounds is available[3], including agonists for neurotransmitter receptors such as glutamate, GABA, acetylcholine and biogenic amines and intracellular messengers such as calcium (in which a chelator of calcium is the molecule caged) and inositol-1,4,5-trisphosphate (IP_3). Uncaging approaches open the possibility of using light to probe semi-intact tissue noninvasively.

Caged compounds are useful whenever control of cellular biochemistry is needed on subsecond time scales. In addition to applications to neurophysiology, caged compounds have been useful in studying other biological problems requiring comparable time resolution such as secretion[5], muscle activation[6], fertilization[7] and nuclear signaling[8]. An intriguing recent advance is the development of a caged inhibitor of protein synthesis[9].

Uncaging light pulses are usually delivered to a single fixed location. To overcome this limitation we have developed a system that rapidly deflects and modulates the uncaging beam using acousto-optical deflectors (AODs). AODs allow extremely rapid access to many locations in tissue and have been used previously in some commercial (Noran Inc.) or custom-built[10,11] imaging systems. Our system uncages at over 20,000 locations per second, considerably faster than older uncaging systems that steer beams with modified galvanometer mirrors and mechanical shutters[12,13]. Here we present the basic physical characteristics of this system and demonstrate its application to several problems in neuroscience.

RESULTS

General system design

Our system design is illustrated in **Figure 1a** and described in detail in the **Supplementary Note** online. The ultraviolet light source is a frequency tripled Nd:YVO_4 laser (DPSS Corp.; 50–60 ns, $\lambda = 355$ nm pulses at a 100-kHz repetition rate with average power >400 mW) whose beam is expanded threefold in diameter and directed through two crosswise-oriented tellurium dioxide (TeO_2) AODs and a two-lens 1:1 telescope into the optical path of a two-photon microscope[14]. The AOD assembly, lenses and an iris are spaced at intervals approximately equal to the lens focal length *f*, thus forming a 4-*f* system. Such an arrangement transfers a beam that pivots around the AOD axis to a pivot point at the back aperture of the objective, thus allowing scanning of the beam in the focal plane[15]. The laser output is gated using its Q-switching control so that output pulses are emitted only after the AOD has settled at a new value. Control pulses set the repetition rate of the laser to be the same as the AOD switching rate. At the resulting pulse rates the energy per pulse is reproducible (s.d. divided by

[1]Department of Molecular Biology, [2]Program in Neuroscience and [3]Department of Physics, Lewis Thomas Laboratory, Washington Road, Princeton University, Princeton, New Jersey 08544, USA. [4]Present address: Faculty of Biomedical Engineering, Technion 32000, Haifa, Israel. [5]These authors contributed equally to this work. Correspondence should be addressed to S.S.-H.W. (sswang@princeton.edu).

RECEIVED 25 MAY; ACCEPTED 22 AUGUST; PUBLISHED ONLINE 21 OCTOBER 2005; DOI:10.1038/NMETH793

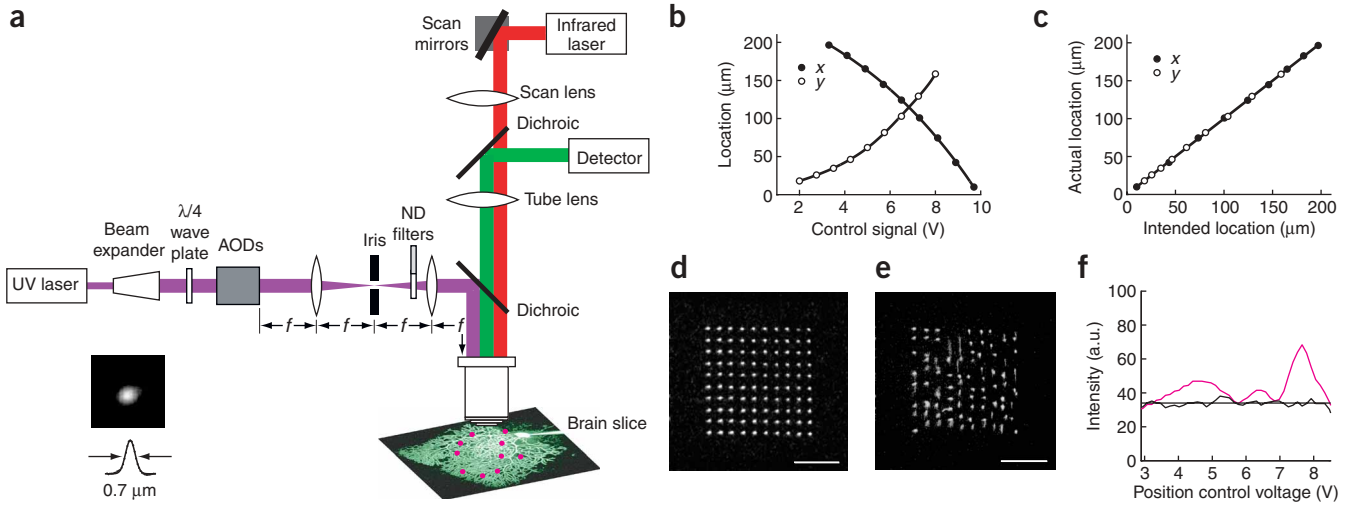

Figure 1 | A system for patterned uncaging and two-photon imaging. (**a**) An ultraviolet uncaging laser beam is projected into the focal plane of a two-photon microscope. The AODs, lenses and iris approximately form a 4-*f* imaging system. The inset shows the lateral resolution of a single uncaging spot. (**b**) Dependence of two-dimensional uncaging location on the control voltage, as measured by uncaging dried fluorescein dextran. The voltages control the frequency of the radio-frequency wave used to excite the two (*x* and *y*) acousto-optic crystals. (**c**) Comparison of the expected and actual uncaging after linearization of the response locations in **b** by a fourth-order polynomial. (**d**) Uncaging pattern at 45-μs access time per point and with adjustments to laser intensity to compensate for position-dependent variations in transmission efficiency. Bar, 50 μm. (**e**) Uncaging pattern for a randomly-accessed grid pattern at 27-μs access time per point. Bar, 50 μm. (**f**) Light energy reaching the specimen at different diffraction angles (magenta) is made more uniform (black) by reducing the first-order beam intensity at angles of higher transmission efficiency.

mean = 2–3%), and is better than the laser manufacturer's specification for the fastest pulse rates.

For steering the ultraviolet laser beam, a radio-frequency shear pressure wave propagating through the two TeO_2 crystals (model 2DS-150-50-.364; Brimrose Corp.) at the corresponding speed of sound (617 m/s) creates periodic variations in refractive index, forming effective gratings that steer the beam. Using the iris, the first-order deflection beam, which contains the most power, is passed while other beams (mixed zero and/or higher-order) are blocked. We chose a shear-mode TeO_2 device over a longitudinal device in which the speed of sound is higher (4,260 m/s). Higher wave speeds potentially shorten switching times but also impose a need for elongated deflectors and relatively complex designs for two-dimensional systems (A. Bullen, V. Iyer, S.S. Patel & P. Saggau, *Soc. Neurosci. Abstr.* **25**, 601.13, 1999; and ref. 16). The transmission of TeO_2 is not as consistent for near-ultraviolet (330–380 nm) light as for visible and infrared light, so crystals were selected by the manufacturer for high transmission. In our system with the AOD power switched off, the two TeO_2 crystals selected transmit ~75% of the entering light. Because light throughput depends on the diffraction efficiency of the AOD, which for our devices depends on the circular polarization of the incoming beam, polarization is adjusted using a quarter-wave plate. After these adjustments the light energy arriving at the specimen is up to 300 nJ per pulse at ~500 mW average laser power. This is reduced to the desired amount of energy with a neutral-density filter wheel and by modulating the radio-frequency power. An aperture is placed in the image plane to block higher diffraction orders as well as the parked beam.

The ultraviolet uncaging beam emerging from the AOD is projected through two lenses and then merged with the infrared imaging beam using a dichroic mirror. Both beams are then directed through a 40× objective (Leica model UVI, 0.8 NA) into a single shared focal plane. To ensure that the focal planes of the ultraviolet and infrared beams were near to one another, we used an objective with good transmittance at both wavelengths (Leica objective model UVI; transmission at 355 nm: ~60%, at 830 nm: ~75%) and wide-band correction for intrinsic variations in the index of refraction. Photolysis can be achieved in a variety of axial positions relative to the image plane by moving the first lens after the AOD along its optical axis to shift the focus of the ultraviolet beam. For most experiments the lens is used to focus uncaging into the same plane as the infrared beam[17].

We visualized uncaging by exciting fluorescent beads or by uncaging dried samples of caged fluorescein dextran. The uncaging focal volume has an approximately Gaussian profile both laterally in the focal plane (0.7-μm full width at half maximum; FWHM), and axially (10-μm FWHM), corresponding to an NA of approximately 0.3. This is less spatial resolution than the focal volume of two-photon excitation (for $\lambda = 830$ nm and NA 0.7, lateral FWHM = 0.4 μm and axial FWHM = 2.6 μm; ref. 18). Further expansion of the uncaging beam entering the AOD introduced more spatial asymmetry in the focal volume and was not done. In brain slices (see **Supplementary Data 1** and **Supplementary Fig. 1** online), because of scattering, the estimated total excitation energy in the focal volume decreased with a length constant of 32 μm. The lateral and axial FWHM of the uncaging spot grew slightly in the first 30 microns of the slice, reaching values of 3 μm (lateral) and 17 μm (axial) at a depth of 25 microns.

Beam steering requires measurement of the relationship between control voltage and uncaging position. We did this by measuring uncaging position for a grid pattern of *x* and *y* control voltages (**Fig. 1b**) and finding mapping functions for interpolation and linearization (**Fig. 1c**). It is possible in this way to reliably access fields of up to ~170 μm × 170 μm.

The fundamental limit of time resolution is the theoretical acousto-optical switching time, $\tau = d_{aperture} / v_{acoustic}$, where $d_{aperture}$ is the diameter of the aperture and $v_{acoustic}$ is the acoustic wave frequency. For a 5-mm transmitted beam diameter, τ is 8 μs. An additional limit is the switching time of the radiofrequency driver, whose nominal switching time was 50 μs (Brimrose model VFE-150-50-V-B1-F2-2Ch, channels: deflection in x and y and intensity in x and y). The long switching time required us to use a switching time between uncaging locations of 40 μs or more (**Fig. 1d**). Faster switching rates resulted in uncaging between the intended locations (**Fig. 1e**).

Each crystal is controlled by two voltages via the radiofrequency acousto-optical driver. One voltage controls the wave frequency between 125 and 175 MHz and directs the first-order diffracted beam over a 1.7-degree range. The second voltage controls the wave amplitude and thus the first-order beam intensity. The diffraction efficiency in AOD crystals varies as a function of diffraction angle, with a multiple-hump structure that results from a design that meets two phase-matching criteria (**Fig. 1f**). To obtain a uniform uncaging intensity we used a two-step procedure. First, we generated a map of the intensity of light using a photodiode placed in front of the objective. Next, because the amount of light per pulse is generally more than sufficient to achieve efficient uncaging, we reduced the second control voltage at regions of high intensity. This truncated the peaks of the intensity distribution and gave a relatively flat field (**Fig. 1f**).

Using caged glutamate to emulate dendritic integration

We applied caged glutamate (MNI-glutamate)[19–21] to single and multiple sites on hippocampal pyramidal neurons in rat brain slices (**Fig. 2**). We measured the zone of receptor activation by moving the uncaging location away from a CA1 pyramidal neuron dendrite (**Fig. 2a**). Responses dropped off to 50% of peak at distances between 1.7 and 2.0 μm from the center (mean ± s.e.m., 1.9 ± 0.1 μm for three branchlets). In the NMDA-type glutamate receptor blocker APV (DL-2-amino-5-phosphonovaleric acid; 100–200 μM), the responses were tightly localized to dendrites, with half-maximal distances of 0.75 to 1.4 μm (1.0 ± 0.1 μm, 7 branchlets; smaller than the distance with no antagonist, one-tailed t test, $P < 0.01$), comparable to the resolution in dendritic shafts of two-photon uncaging[22]. As uncaging was done over dendrites and not spines, these responses were likely to include extrasynaptic receptors. Further addition of the non-NMDA receptor antagonist 6,7-dinitroquinoxaline-2,3-dione (DNQX) totally abolished the responses. At single locations, response amplitudes at 10-s intervals were stable over periods of at least 200 s, indicating that responses can be measured repeatedly without cumulative phototoxicity.

To test if patterned uncaging can be used to study signal integration along dendrites, we photolyzed glutamate at ten dendritic locations in rapid succession. Individual responses were small in both current clamp (1–2 mV; **Fig. 2c**) and voltage clamp (7–15 pA), comparable with unitary synaptic transmission events at

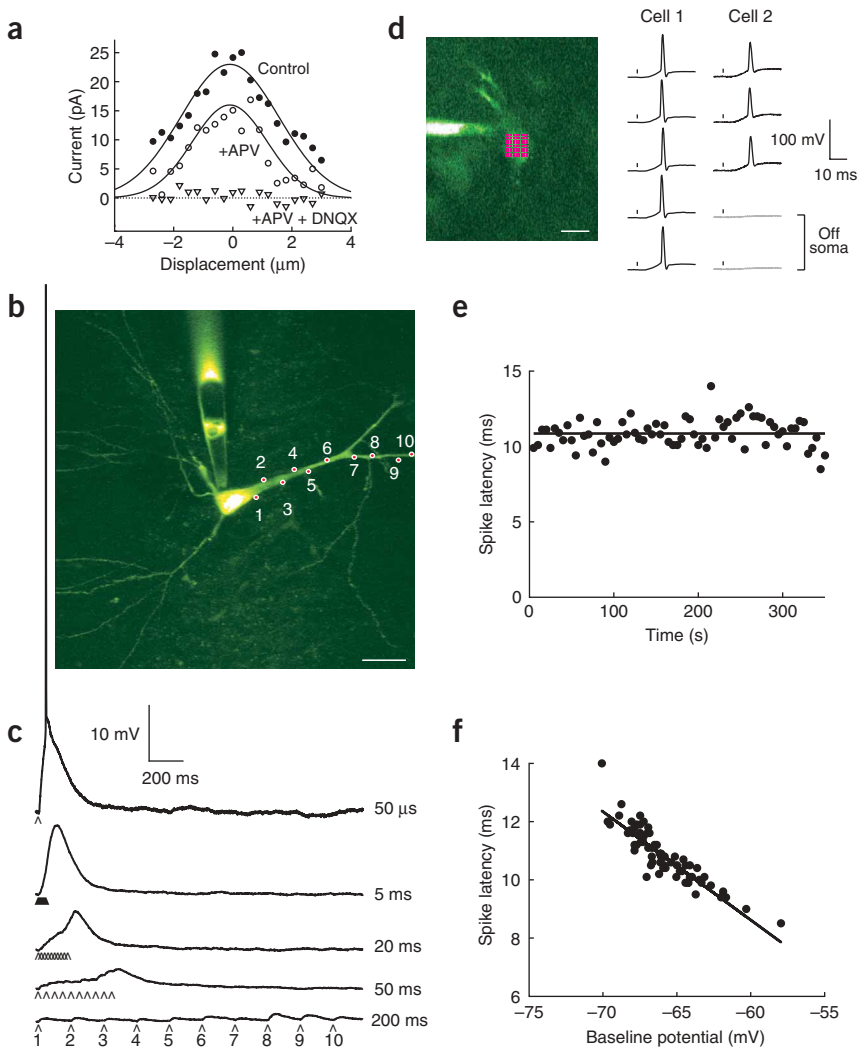

Figure 2 | Using patterned uncaging to emulate dendritic integration. (**a**) Response size as a function of distance from a CA1 basal dendrite. APV (100 μM) reduced the responses by 30% and sharpened the spatial profile of response size. Addition of DNQX (20 μM) abolished the responses. Displacement distance was measured from the center of the dendritic shaft. (**b**) Two-photon image of a CA1 pyramidal neuron showing sequential uncaging locations on the apical dendrite (numbers 1–10). Bar, 20 μm. (**c**) Dendritic integration of uncaging responses from the ten locations shown in **b**. The interval between flashes varied from 50 μs to 200 ms. The subthreshold traces are averages of 3–7 trials. (**d**) Uncaging in a grid pattern (red) over the soma of a CA3 pyramidal cell (two-photon image at left; scale bar, 20 μm) triggers action potentials (first column of traces); five consecutive responses are shown. The second column shows action potentials from a second CA3 cell and two responses (gray) recorded with the grid moved 30 μm away from the soma. The within-grid interval between flashes was 50 μs. (**e**) Latency to the action potential for 68 consecutive responses from the cell in **d**. (**f**) The latency depends on resting potential (same cell as in **d**).

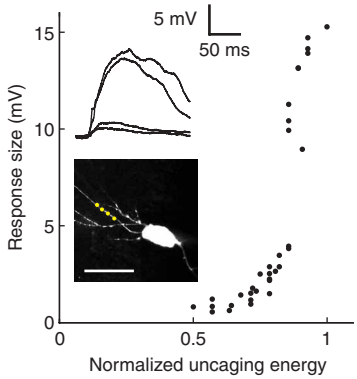

Figure 3 | Local amplification of glutamate responses in pyramidal neuron dendrites. Voltage responses to uncaging increase with increasing pulse energy smoothly at first, with a sharp discontinuity at moderate flash energy (top inset, two example sweeps at low energy and two at high energy). Uncaging was done at four locations (indicated by yellow dots) at once on a single branchlet (lower inset; bar, 50 μm).

CA3-CA1 synapses (5–80 pA)[23]. When responses were evoked at all locations in rapid succession (less than 2 ms between pulses), responses recorded at the soma could sum to reach firing threshold (**Fig. 2b**,**c**).

To explore how precisely action potentials could be triggered, we used rectangular patterns of uncaging spots (9 × 9, spaced at 1.8- to 4.5-micron intervals; 170–600 μM MNI-glutamate, three grid patterns in two recordings). Responses ranged from subthreshold to several spikes. With adjustment of flash intensity, generally within a threefold range, we could evoke one action potential per flash (**Fig. 2d**), a degree of response precision not previously achieved with uncaging. Action potentials occurred within a 3-ms range (**Fig. 2e**; s.d. of spike time, 0.6–1.2 ms); the timing depended on the neuron's resting potential (**Fig. 2f**). When the uncaging pattern was moved by 30 or 80 microns off the soma, no spikes were evoked (mean responses 4.5 mV and 0.8 mV, respectively).

Integration of distributed and complex uncaging patterns

Dendrites can regeneratively amplify synaptic input[1,24]. To assay this local amplification, we uncaged at four locations at once on a basal dendrite. As we increased the energy delivered in each pulse, the response amplitude at first increased gradually. At a threshold of uncaging energy, the reponses jumped suddenly in size (**Fig. 3**), a hallmark of regenerative amplification.

Because realistic spatial input patterns are distributed over time, we applied uncaging sequences to dozens of locations distributed over a dendritic arbor (**Fig. 4**). We selected points using a fluorescence image of the dendrite as a guide. Up to 50 points could be conveniently selected manually in the first minutes of the recording. The sequence of activation, during which all three dendrites receive light pulses, is indicated by the tick marks (**Fig. 4a**,**b**) and in videos available online (**Supplementary Video 1** online). In voltage clamp, current responses to patterned stimulation were reproducible with multiple repetitions of the same sequence, and were different when different activation sequences were used with the same average rate. Similarly, when neurons were allowed to spike freely in current clamp, patterned activation evoked a sequence of action potentials with similar timing from trial to trial.

We quantified the similarity between uncaging responses as the crosscorrelation between pairs of responses evoked in voltage clamp. We calculated correlation coefficients using responses that were mean-subtracted by the average of all responses across three cells. Responses to the same activation pattern given repeatedly were highly correlated (median $r = +0.86$, 25–75% interquartile range +0.69 to +0.92; 224 comparisons between pairs of traces taken from 490 responses in three cells with 8–100 uncaging patterns each; Kolmogorov-Smirnov-test, $P < 0.001$; **Fig. 4c**). In contrast, responses to different activation patterns were uncorrelated (median $r = +0.05$, 25–75% interquartile range –0.61 to +0.65; 20,964 comparisons among 490 responses in three cells; **Fig. 4c**). Thus patterned activation can reproducibly emulate complex signal integration events spanning the dendritic arbor.

To test the ability of the system to uncage and monitor fluorescence signals simultaneously, we measured Ca^{2+} release responses to patterned release of caged IP_3 in rat cerebellar Purkinje neurons (**Supplementary Data 2**, **Supplementary Fig. 2** and **Supplementary Video 2** online).

Using caged glutamate to activate many neurons at once

Glutamate uncaging has been used to identify synaptic connections[4,25] by generating action potentials in presynaptic neurons and searching for postsynaptic responses. The spatial and temporal performance of our uncaging system potentially allowed us to activate multiple presynaptic neurons at once (**Fig. 5**). A cerebellar Purkinje neuron filled with dye and the presynaptic granule cell

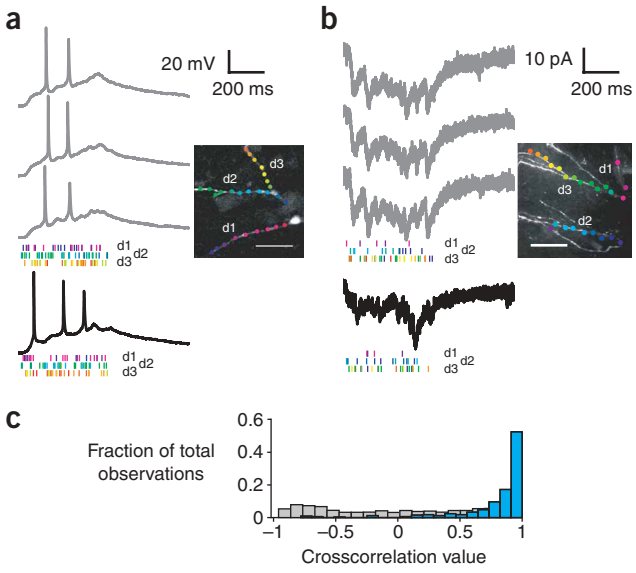

Figure 4 | Repeatability of responses to patterned activation of multiple dendrites. (**a**,**b**) The uncaging locations, distributed over three dendritic branches (d1, d2 and d3), are shown as colored dots on two-photon images of CA1 pyramidal cells. Bars, 20 μm. In current clamp (27 points, 6 Hz average rate) the same sequence of flashes (as indicated by the three tick rasters) evoked a reproducible response (top three traces), but a different pattern with the same average rate (bottom) gave a different response (**a**). Responses in voltage clamp (24 points, 4 Hz); the tick colors in the rasters correspond to the uncaging locations in the inset (**b**). (**c**) Histograms of crosscorrelations between voltage-clamp responses to the same pattern (blue) or different patterns (gray).

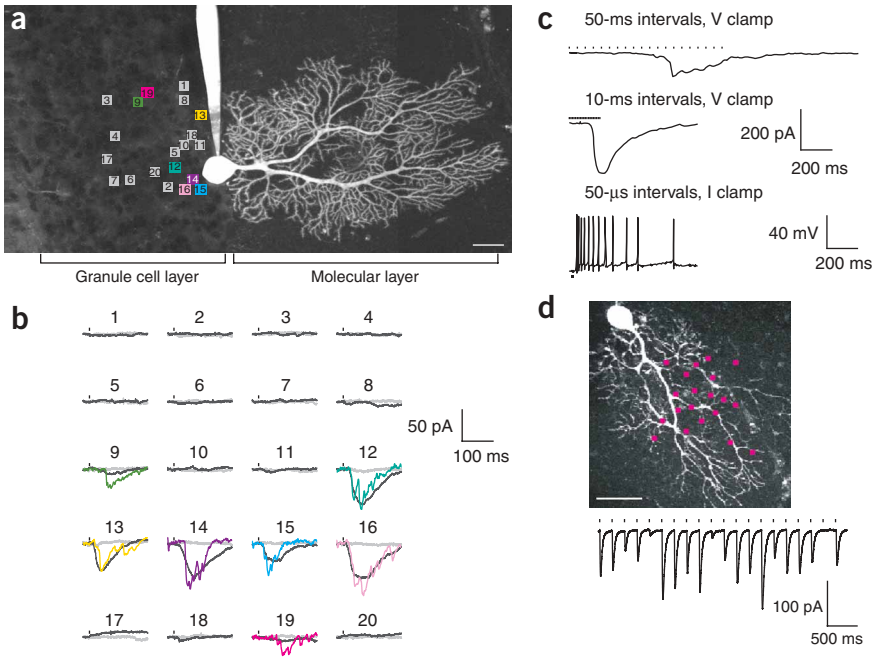

Figure 5 | Patterned activation of presynaptic cells. (**a**) Maximum intensity projection of a postsynaptic cerebellar Purkinje neuron filled via patch clamp recording electrode with fluorescent dye. The squares indicate the positions of 20 uncaging locations in the presynaptic granule cell layer. The locations were visited in the numbered order. Bar, 25 µm. (**b**) Postsynaptic voltage-clamp responses to uncaging at the locations shown in **a**, with 200-ms interlocation intervals. Vertical marks indicate times of uncaging. Shown in gray at each location are responses after addition of APV (400 µM) and lidocaine (500 µM). Also shown (colored traces) are single example traces. (**c**) The same sequence of uncaging locations as **b**, but with interlocation intervals of 50 ms (top), 10 ms (middle) or 50 µs (bottom, in current clamp). (**d**) Twenty uncaging locations over a Purkinje cell dendritic arbor (top; bar 20 µm) were visited at 200 ms inter-grid intervals in the presence of 500 µM lidocaine. Voltage clamp responses from the Purkinje cell (bottom).

layer in negative stain using a small concentration of fluorescent dye is shown in **Figure 5a**. At each of 20 randomly selected locations, uncaging was done at a 3 × 3 array of points spaced at 1.3–2.0 µm intervals. We measured response amplitudes in individual traces over a time window 70–90 ms after the pulse, and defined a *t* score for each location as the mean response divided by the standard error of the mean. We scored locations with $t > 2$ as responding (**Fig. 5b**).

At each responding location ($n = 18$ locations in four recordings, 718 responses total), averaged responses (**Fig. 5b**) had short onset delays from the first uncaging flash (latency 12.6 ± 10.2 ms, mean ± s.d.) and peak amplitudes of 1–54 pA (mean: 19 pA, 25–75% interquartile range 7–28 pA). Responses were completely eliminated by addition of the sodium channel blocker lidocaine (**Fig. 5b**), which prevents propagation of action potentials. Lidocaine did not affect responses to uncaging pulses delivered directly to the Purkinje cell dendritic arbor (**Fig. 5d**). Thus, photolyzed glutamate triggered action potentials in granule cells and synaptic responses in Purkinje cells.

Our EPSC amplitudes are comparable to measurements made from unitary granule cell–Purkinje cell pairs (compare with 2–60 pA, mean 14 pA in ref. 26). Multiple rising phases could often be seen in individual responses (**Fig. 5b**), suggesting that multiple granule cells might have been activated at once. But when the granule layer stimulus pattern was shifted 3 µm laterally, individual Purkinje cell responses were reduced by at least half in 72% of movements, across eight responding locations, favoring the possibility that the multiple rising phases were caused by single granule cells firing bursts[27,28]. Finally, we tested whether granule cell–Purkinje cell responses could summate, by activating all twenty sites at once in 9 ms. This triggered a burst of spikes in the Purkinje cell (**Fig. 5c**; $n = 4$ cells).

DISCUSSION

We have developed a system that allows stimulation of neural structures in complex spatial and temporal patterns. The system allows uncaging at submicron resolution with a maximal uncaging rate of over 20,000 locations per second. Our work opens the possibility of investigating how neurons integrate signals resulting from rapidly changing, complex activity conditions that until now have not been explored *in vitro*.

Our system's spatial resolution is well-suited for studying integration in whole dendrites and neurons, in which signals are integrated on length scales of tens to hundreds of microns. Compared with patterned two-photon uncaging using infrared lasers, our implementation has the advantages of design simplicity, the use of many caged compounds now available with good one-photon cross-section, and the reduced cost of the uncaging laser. These advantages make our approach an attractive choice for micron-level spatial performance.

Improved spatial resolution can be achieved by reducing AOD-induced distortions that limit the system's effective numerical aperture or by expanding the beam after the AODs to fill the back aperture of the microscope objective. For three-dimensional control of uncaging, fast control of the axial position may be accomplished using a piezoelectric focusing device that fits between the microscope turret and objective (see, for example, http://www.physikinstrumente.de) and allows travel of hundreds of microns on the time scale of tens of milliseconds. Another option is the use of a variable-focus lens. Temporal resolution, which in our system is limited by the AOD driver, can potentially be improved up to fivefold by using a faster voltage-controlled oscillator. Future improvements in both spatial and temporal resolution will be needed for studies in which single-spine resolution is critical.

Patterned uncaging can be applied to the study of synaptic plasticity, which is thought to provide a substrate for the initial stages of learning and memory. Uncaging has been used to induce long-term depression and potentiation at single sites[13,29–31]. Similarly, assessing the dependence of synaptic plasticity on the timing of single spikes[32] and the location of the synaptic input[33] has required pooling data from dozens of neuronal recordings taken with great effort over a period of months. Patterned uncaging may

provide a high-throughput assay for synaptic plasticity that allows rapid measurement of how timing-dependent and location-dependent postsynaptic learning rules can vary as a function of complex spatiotemporal activity patterns[34]. We have demonstrated multisite activation at dozens of sites on a dendritic arbor; in the future, selection of larger numbers of points should be possible with the help of automated feature recognition[35].

Most photolysis work to date in dendrites has used caged glutamate, leaving open many possibilities using other neurotransmitters. Complex activity patterns have been observed in neurons that secrete other transmitters, including some often thought of as neuromodulators[36]. This temporal complexity suggests that the ability to rapidly generate complex patterns of these neurotransmitters will lead to new insights on how they participate in signal integration on fast time scales.

Our system can activate many presynaptic neurons in precise spiking patterns to allow fast mapping of local[12] and distributed[37] neural circuits. The ability to activate many neurons in a preparation may be of use in the development of prosthetic neural interfaces[38]. In summary, the introduction of patterned neurotransmitter uncaging to emulate neural activity opens new windows into study of the integration of distributed signals by dendrites and neuronal networks.

METHODS

Slice preparation and electrophysiology. We prepared transverse hippocampal slices and sagittal cerebellar slices from anesthetized 13–21-day-old Sprague-Dawley rats in accordance with procedures approved by the Princeton University Institutional Animals Care and Use Committee. We cut slices in ice-cold artificial cerebrospinal fluid (ACSF) comprising 126 mM NaCl, 3 mM KCl, 1 mM NaH_2PO_4, 25 mM D-glucose, 25 mM $NaHCO_3$, 2 mM $CaCl_2$ and 1 mM $MgCl_2$ (osmotic strength: 320 mOsm) saturated with 95% O_2–5% CO_2, incubated the slices at 34 °C (hippocampal slices, 10–15 min; cerebellar slices, 45 min), and transferred the slices to a 20–23 °C interface (hippocampal) or submersion (cerebellar) chamber. At least 1 h after slicing, we transferred the slices to a recording chamber in the patterned uncaging system and perfused the slices at 2-4 ml/min with room-temperature ACSF bubbled with 95% O_2–5% CO_2. We made whole-cell patch recordings (current-clamp and voltage-clamp) using 2–5 MΩ pipettes filled with solution containing 0.02–0.05 mM Alexa 488 hydrazide (Molecular Probes), 133 mM methanesulfonic acid, 7.4 mM KCl, 0.3 mM $MgCl_2$, 3 mM Na_2ATP, 0.3 mM Na_2GTP, 10 mM NaHEPES, pH to 7.3 with KOH (290 mOsm). We performed recordings with a BVC 700A (Dagan) or an Axopatch 200B (Axon Instruments) patch clamp amplifier and a data acquisition board (National Instruments model PCI-MIO-16E-4). A custom LabView program (National Instruments) controlled experiments and provided unified control of the AODs and the electrophysiology apparatus. We delivered MNI-caged glutamate (Tocris or Sigma-Aldrich) either locally near the imaged neuron through a 50 μm inner diameter capillary tube (5 mg/ml ≈13 mM), or in the bath at 140–170 μM.

We uncaged glutamate using one pulse of light per location, except in one CA3 pyramidal cell experiment (**Fig. 2d**) in which we gave two pulses per location and six experiments from **Supplementary Figure 1** in which we gave 2–3 pulses. In hippocampal NMDA receptor block experiments, we applied 200 μM APV through the capillary in all but one experiment, in which we applied 100 μM APV in the bath. In **Fig. 5**, we applied 10 μM bicuculline (0.01% DMSO) in the bath to block inhibition.

Note: Supplementary information is available on the Nature Methods website.

ACKNOWLEDGMENTS

This work was supported by grants from the Princeton Center for Photonics and Optoelectronic Materials, the US National Institutes of Health, the National Science Foundation (NSF), and the W.M. Keck Foundation to S.S.-H.W., a Lewis Thomas fellowship to S.S., an NSF Graduate Research Fellowship to D.H.O. and a Burroughs-Wellcome Interfaces of Science fellowship to D.V.S. We thank J. Soos from Brimrose Corp. for designing the AOD device and K. Visscher, M. McDonald, J. Puchalla, G. Wittenberg, G. Major and T. Adelman for advice and discussion.

COMPETING INTERESTS STATEMENT

The authors declare that they have no competing financial interests.

Published online at http://www.nature.com/naturemethods/
Reprints and permissions information is available online at http://npg.nature.com/reprintsandpermissions/

1. Polsky, A., Mel, B.W. & Schiller, J. Computational subunits in thin dendrites of pyramidal cells. *Nat. Neurosci.* **7**, 621–627 (2004).
2. London, M. & Segev, I. Synaptic scaling *in vitro* and *in vivo*. *Nat. Neurosci.* **4**, 853–855 (2001).
3. Adams, S.R. & Tsien, R.Y. Controlling cell chemistry with caged compounds. *Annu. Rev. Physiol.* **55**, 755–784 (1993).
4. Callaway, E.M. & Yuste, R. Stimulating neurons with light. *Curr. Opin. Neurobiol.* **12**, 587–592 (2002).
5. Heidelberger, R., Heinemann, C., Neher, E. & Matthews, G. Calcium dependence of the rate of exocytosis in a synaptic terminal. *Nature* **371**, 513–515 (1994).
6. DelPrincipe, F., Egger, M. & Niggli, E. Calcium signalling in cardiac muscle: refractoriness revealed by coherent activation. *Nat. Cell Biol.* **1**, 323–329 (1999).
7. Jones, K.T. & Nixon, V.L. Sperm-induced Ca^{2+} oscillations in mouse oocytes and eggs can be mimicked by photolysis of caged inositol 1,4,5-trisphosphate: evidence to support a continuous low level production of inositol 1,4,5-trisphosphate during mammalian fertilization. *Dev. Biol.* **225**, 1–12 (2000).
8. Echevarría, W., Leite, M.F., Guerra, M.T., Zipfel, W.R. & Nathanson, M.H. Regulation of calcium signals in the nucleus by a nucleoplasmic reticulum. *Nat. Cell Biol.* **5**, 440–446 (2003).
9. Goard, M. *et al.* Light-mediated inhibition of protein synthesis. *Chem. Biol.* **12**, 685–693 (2005).
10. Bullen, A., Patel, S.S. & Saggau, P. High-speed, random-access fluorescence microscopy: I. High-resolution optical recording with voltage-sensitive dyes and ion indicators. *Biophys. J.* **73**, 477–491 (1997).
11. Saggau, P., Bullen, A. & Patel, S.S. Acousto-optic random-access laser scanning microscopy: fundamentals and applications to optical recording of neuronal activity. *Cell Mol. Biol.* **44**, 827–846 (1998).
12. Shepherd, G.M., Pologruto, T.A. & Svoboda, K. Circuit analysis of experience-dependent plasticity in the developing rat barrel cortex. *Neuron* **38**, 277–289 (2003).
13. Matsuzaki, M., Honkura, N., Ellis-Davies, G.C.R. & Kasai, H. Structural basis of long-term potentiation in single dendritic spines. *Nature* **429**, 761–766 (2004).
14. Denk, W., Strickler, J.H. & Webb, W.W. Two-photon laser scanning fluorescence microscopy. *Science* **248**, 73–76 (1990).
15. Tsai, P.S. *et al.* Principles, design and construction of a two-photon laser-scanning microscope for *in vitro* and *in vivo* studies. In *In vivo optical imaging of brain function* (ed. Frostig, R.D.) 113–171 (CRC Press, Boca Raton, Florida, USA, 2002).
16. Iyer, V., Losavio, B.E. & Saggau, P. Compensation of spatial and temporal dispersion for acousto-optic multiphoton laser-scanning microscopy. *J. Biomed. Opt.* **8**, 460–471 (2003).
17. Bliton, A.C. & Lechleiter, J.D. Optical considerations at ultraviolet wavelengths in confocal microscopy. In *Handbook of biological confocal microscopy* (ed. Pawley, J.B.) 431–444 (2nd edn.Plenum Press, New York, 1995).
18. Brown, E. & Webb, W. Two-photon activation of caged calcium with submicron, submillisecond resolution. in *Caged Compounds. Methods of Enzymology*. (ed. Marriott, G.) **291**, 356–380 (Academic Press, San Diego, 1998).
19. Papageorgiou, G. & Corrie, J.E.T. Effects of aromatic substituents on the photocleavage of 1-acyl-7-nitroindolines. *Tetrahedron* **56**, 8197–8205 (2000).

20. Canepari, M., Nelson, L., Papageorgiou, G., Corrie, J.E. & Ogden, D. Photochemical and pharmacological evaluation of 7-nitroindolinyl- and 4-methoxy-7-nitroindolinyl-amino acids as novel, fast caged neurotransmitters. *J. Neurosci. Methods* **112**, 29–42 (2001).
21. Matsuzaki, M. *et al.* Dendritic spine geometry is critical for AMPA receptor expression in hippocampal CA1 pyramidal neurons. *Nat. Neurosci.* **4**, 1086–1092 (2001).
22. Smith, M.A., Ellis-Davies, G.C. & Magee, J.C. Mechanism of the distance-dependent scaling of Schaffer collateral synapses in rat CA1 pyramidal neurons. *J. Physiol. (Lond.)* **548**, 245–258 (2003).
23. O'Connor, D.H., Wittenberg, G.M. & Wang, S.S-H. Graded bidirectional synaptic plasticity is composed of switch-like unitary events. *Proc. Natl. Acad. Sci. USA* **102**, 9679–9684 (2005).
24. Schiller, J. & Schiller, Y. NMDA receptor-mediated dendritic spikes and coincident signal amplification. *Curr. Opin. Neurobiol.* **11**, 343–348 (2001).
25. Callaway, E.M. & Katz, L.C. Photostimulation using caged glutamate reveals functional circuitry in living brain slices. *Proc. Natl. Acad. Sci. USA* **90**, 7661–7665 (1993).
26. Barbour, B. Synaptic currents evoked in Purkinje cells by stimulating individual granule cells. *Neuron* **11**, 759–769 (1993).
27. Chadderton, P., Margrie, T.W. & Häusser, M. Integration of quanta in cerebellar granule cells during sensory processing. *Nature* **428**, 856–860 (2004).
28. Isope, P., Franconville, R., Barbour, B. & Ascher, P. Repetitive firing of rat cerebellar parallel fibres after a single stimulation. *J. Physiol. (Lond.)* **554**, 829–839 (2004).
29. Kandler, K., Katz, L.C. & Kauer, J.A. Focal photolysis of caged glutamate produces long-term depression of hippocampal glutamate receptors. *Nat. Neurosci.* **1**, 119–123 (1998).
30. Dodt, H., Eder, M., Frick, A. & Zieglgansberger, W. Precisely localized LTD in the neocortex revealed by infrared-guided laser stimulation. *Science* **286**, 110–113 (1999).
31. Eder, M., Zieglgansberger, W. & Dodt, H.U. Neocortical long-term potentiation and long-term depression: site of expression investigated by infrared-guided laser stimulation. *J. Neurosci.* **22**, 7558–7568 (2002).
32. Abbott, L.F. & Nelson, S.B. Synaptic plasticity: taming the beast. *Nat. Neurosci.* **3**, 1178–1183 (2000).
33. Froemke, R.C., Poo, M-m. & Dan, Y. Spike-timing-dependent synaptic plasticity depends on dendritic location. *Nature* **434**, 221–225 (2005).
34. Stuart, G.J. & Häusser, M. Dendritic coincidence detection of EPSPs and action potentials. *Nat. Neurosci.* **4**, 63–71 (2001).
35. Koh, I.Y., Lindquist, W.B., Zito, K., Nimchinsky, E.A. & Svoboda, K. An image analysis algorithm for dendritic spines. *Neural Comput.* **14**, 1283–1310 (2002).
36. Hyland, B.I., Reynolds, J.N., Hay, J., Perk, C.G. & Miller, R. Firing modes of midbrain dopamine cells in the freely moving rat. *Neuroscience* **114**, 475–492 (2002).
37. Brivanlou, I.H., Dantzker, J.L., Stevens, C.F. & Callaway, E.M. Topographic specificity of functional connections from hippocampal CA3 to CA1. *Proc. Natl. Acad. Sci. USA* **101**, 2560–2565 (2004).
38. Horch, K.W. & Dhillon, G.S. (eds.). *Neuroprosthetics: theory and practice* (World Scientific, New Jersey, 2004).